Carbon Nanotubes in Water: Structural Characteristics and Energetics

J. H. Walther,[†] R. Jaffe,[‡] T. Halicioglu,[§] and P. Koumoutsakos*,[||]

Institute of Computational Sciences, ETH Zentrum, WET D5, Weinbergstrasse 43, CH-8092 Zurich, Switzerland, NASA Ames Research Center, Moffett Field, California 94035, Eloret Corporation, 690 West Fremont Avenue, Sunnyvale, California, and Center for Turbulence Research, NASA Ames/Stanford University, Moffett Field, California 94035

Received: April 10, 2001; In Final Form: July 6, 2001

We study the structural properties of water surrounding a carbon nanotube using molecular dynamics simulations. The interaction potentials involve a description of the carbon nanotube using Morse, harmonic bending, torsion, and Lennard-Jones potentials. The water is described by the flexible Simple Point Charge (SPC) model by Teleman et al.,[1] and the carbon−water interactions include a carbon−oxygen Lennard-Jones potential, and an electrostatic quadrupole moment acting between the carbon atoms and the charge sites of the water. Vibration of the breathing mode of the carbon nanotube in water is inferred from the oscillations in carbon−carbon van der Waals energy, and the inverse proportionality between the radius of the carbon nanotube and the breathing frequency is in good agreement with experimental values. The results indicate, that under the present conditions, the presence of the water has a negligible influence on the breathing frequency. The water at the carbon−water interface is found to have a HOH plane nearly tangential to the interface, and the water radial density profile exhibits the characteristic layering also found in the graphite−water system. The average number of hydrogen bonds decreases from a value of 3.73 in the bulk phase to a value of 2.89 at the carbon−water interface. The inclusion of the carbon quadrupole moment is found to have a negligible influence on the structural properties of the water. Energy changes that occur by the process of introducing a carbon nanotube in water are calculated. The creation of a cavity in the bulk water to accommodate the nanotube constitutes the largest energy contribution. Results include an analysis of surface structure and energy values for planar and for concave cylindrical surfaces of water.

1. Introduction

The unique mechanical and electrical properties of carbon nanotubes (CNT)[2] have prompted studies of their application in a number of fields including biosensors,[3] atomic force microscopy,[4−6] and fuel storage.[7−10] A common aspect of these applications is the interaction of the CNT with the surrounding medium, and in particular the hydrophobic−hydrophilic behavior of the CNT. Since a single-wall carbon nanotube consists of a graphene sheet rolled up to form a tube, we expect that the properties of CNT−water interface to be similar to those of the graphite−water interface to first order. The latter is known to be strongly hydrophobic,[11] and to exhibit a preferred orientation of the water dipole moment tangential to the interface.[12−14] However, most of the modeling studies have been conducted for idealized geometries and interaction potentials, and for planar interfaces, but not for graphite-water interfaces with convex geometries, such as those exterior to carbon nanotubes.

The wetting properties of carbon nanotubes were found to depend on the surface tension (γ) of the fluid, with a threshold value of 100−200 mN/m indicating that water ($\gamma = 72$ mN/m) should wet carbon nanotubes.[15,16]

Nevertheless, carbon nanotubes are generally found to be insoluble in most common solvents,[17,18] including water. However, they can be made soluble with the aid of surfactants,[19] by adding hydrophilic groups (aliphatic amines) to open ends of the tubes,[20,21] or by fluoridating their side walls.[22]

In the present study we examine the structural properties of water surrounding a (16,0) carbon nanotube by performing detailed, fully atomistic molecular dynamics simulations of a 12.52 Å diameter zigzag carbon nanotube in water. The carbon nanotube is described by Morse stretch, harmonic bend, torsion, and Lennard-Jones potentials, and the water by the flexible SPC model of Teleman et al.[1] The carbon−water interaction is described by a carbon−oxygen van der Waals relation augmented with a carbon quadrupole moment−water partial charge interaction, as suggested by Vernov and Steele,[23] and by Marković et al.[24,25] In our study, we consider the structure of the CNT−water interface including modification of the water hydrogen bond structure as well as the energetics of the water in the presence of the carbon nanotube.

The remainder of this paper is organized as follows: Section 2 describes the potentials and numerical method, Section 3 presents the results of the simulations, and a summary is provided in Section 4.

2. Method of Calculation

The carbon nanotube−water system is modeled using classical molecular dynamics simulations in the microcanonical (NVE) ensemble subject to periodic boundary conditions in all spatial directions. Thus, in the present study the carbon nanotube represents an infinitely long tube, and end-effects induced by the caps are neglected. Due to their usually large length-to-

* Corresponding author.
[†] Institute of Computational Science, ETH Zentrum.
[‡] NASA Ames Research Center, Moffett Field.
[§] Eloret Corporation.
[||] Center for Turbulence Research, NASA Ames/Stanford University.

10.1021/jp011344u CCC: $20.00
Published on Web 09/21/2001

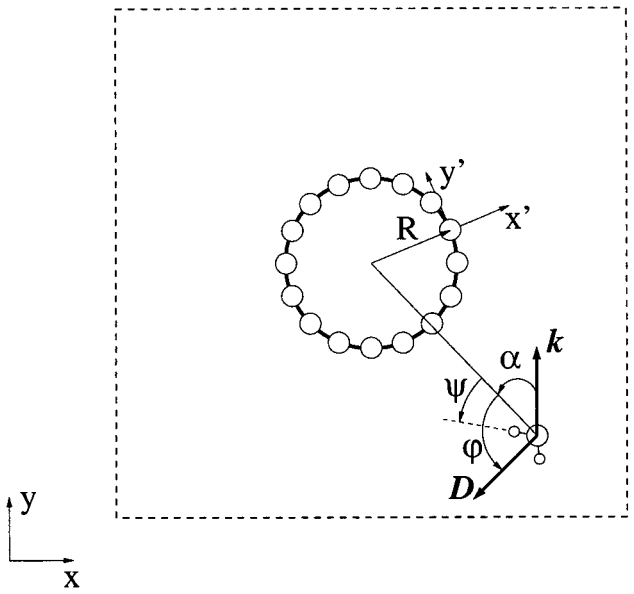

Figure 1. Schematic of the CNT−water system. R denotes the radius of the carbon nanotube, *D* the water dipole moment, and *k* the plane of the water molecule. (x', y') is the local coordinate system used in the calculation of the quadrupole interactions. The orientation of the water molecules is given in terms of the angles φ, ψ, and α. The dashed box indicates the location of the periodic boundary.

diameter ratio, the error introduced by this approximation is expected to be insignificant. The water is described by the flexible SPC model[1] featuring harmonic stretch and bend terms between the oxygen and hydrogen atoms, that also hold the partial charges.

The high-frequency oscillations encountered using flexible water models are of the order of 3500 cm^{-1} which are somewhat larger than the CNT vibrational modes of 1500 cm^{-1}.[26] Hence, for this case, the use of the flexible water model imposes a slightly more restrictive requirement for the choice of time step size compared to rigid water models. A time step (δt) of 0.2 fs proved sufficient for stability of the trajectory and conservation of energy, and has been used throughout.

The water molecules are initially placed on a regular lattice and the system is equilibrated to obtain the desired temperature (T) of 300 K, and the water bulk density (ρ_0) of 997 kg m^{-3}. Temperature control is achieved by velocity scaling imposed every 0.1 ps, and the control is switched off after the equilibration phase at 4 ps. Since the initial placement of the atoms does not allow an accurate predetermination of the bulk water density in the vicinity of the nanotube, the volume of the computational box is adjusted in the equilibration phase to match the target bulk density of the water. The regulation of the volume is performed by repositioning the periodic boundary in the ***x***- and ***y***-planes (see Figure 1) while keeping the length of the box in the ***z***-direction fixed. This procedure prevents any deformation of the carbon nanotube during the volume adjustment.

2.1. Potential Functions. *2.1.1. Carbon−Carbon Interactions.* The carbon nanotube is modeled by terms describing Morse bond, harmonic cosine of the bending angle, and a 2-fold torsion potential as

$$U(r_{ij},\theta_{ijk},\phi_{ijkl}) = K_{Cr}(\xi_{ij}-1)^2 + \frac{1}{2}K_{C\theta}(\cos\theta_{ijk}-\cos\theta_C)^2 + \frac{1}{2}K_{C\phi}(1-\cos 2\phi_{ijkl}) \quad (1)$$

where

$$\xi_{ij} = e^{-\gamma(r_{ij}-r_C)} \quad (2)$$

and θ_{ijk} and ϕ_{ijkl} represent all the possible bending and torsion angles, and r_{ij} represents all the distances between bonded atoms. K_C, $K_{C\theta}$, and $K_{C\phi}$ are the force constants of the stretch, bend, and torsion potentials, respectively, and r_C, θ_C, and ϕ_C the corresponding reference geometry parameters for graphene. The Morse stretch and angle bending parameters were first given by Guo et al.[27] and subsequently used by Tuzun et al.[28] These parameters, listed in Table 1, were originally derived to describe the geometry and phonon structure of graphite and fullerene crystals.

The torsion term is needed to provide a measure of the strain due to curvature of the reference graphene sheet. This curvature strain prevents collapse of the nanotube and imparts stiffness with respect to bending deformations. To obtain a physically reasonable torsion parameter, quantum chemistry calculations were carried out for planar and curved tetracene ($C_{18}H_{12}$) which consists of 4 hexagonal rings fused together in a strip like part of the circumference of a zigzag carbon nanotube. The calculations were carried out using the Gaussian98 software package.[29] Tetracene is planar with a 9.778 Å separation between the C−C bonds on opposite ends of the molecule. If the tetracene molecule were extracted from a (16, 0) nanotube and held rigid, that end-to-end separation would be 8.795 Å. Quantum chemistry calculations were carried out using density functional theory (DFT) with the hybrid nonlocal B3LYP functional[30] as implemented in the Gaussian98 software package. For each amount of curvature, the molecular geometry was completely optimized except for the end-to-end distance constraint. The energy difference between the curved and planar tetracene molecules (ΔE_{curv}) was determined to be 71.11 kJ mol^{-1} using the standard 6-31G(d) contracted Gaussian atomic orbital basis set. The curvatures considered were appropriate for (n, 0) nanotubes with n ranging from 12 to 24. The torsion parameter $K_{C\phi}$ was determined from

$$K_{C\phi} = 2\Delta E_{curv}\left(\sum_{i}^{84} 1-\cos 2\phi_i\right)^{-1} \quad (3)$$

with the summation over the complete set of 84 torsion angles in the optimized curved tetracene molecule (four for each C−C bond). For all cases studied, $K_{C\phi}$ was between 24.60 and 25.25 kJ mol^{-1}. The value of 25.12 kJ mol^{-1} was selected for the present study.

A Lennard-Jones term is added to the nanotube potential to account for the steric and van der Waals carbon−carbon interaction

$$U(r_{ij}) = 4\epsilon_{CC}\left[\left(\frac{\sigma_{CC}}{r_{ij}}\right)^{12} - \left(\frac{\sigma_{CC}}{r_{ij}}\right)^{6}\right] \quad (4)$$

excluding 1−2 and 1−3 pairs, and the parameters ϵ_{CC} and σ_{CC} are taken from the so-called Universal Force Field (UFF),[31] cf. Table 1.

2.1.2. Model Potential for Water. The flexible SPC water model by Teleman et al.[1] is described by intramolecular harmonic stretching and bending between the hydrogen and oxygen atoms as

$$U(r_{ij},\theta_{ijk}) = \frac{1}{2}K_{Wr}(r_{ij}-r_W)^2 + \frac{1}{2}K_{W\theta}(\theta_{ijk}-\theta_W)^2 \quad (5)$$

where K_{Wr} and $K_{W\theta}$ are the parameters of the potential, and r_W and θ_W the reference bond length (1.0 Å) and angle (109.47°),

TABLE 1: Parameters for the Carbon Interaction Potentials[a] (K_{Cr}, r_C, and γ are the parameters of the Morse potential, $K_{C\theta}$ and θ_C the angle parameters, and $K_{C\phi}$, is the torsion parameter; ϵ_{CC} and σ_{CC} are the Lennard-Jones parameters for the carbon−carbon interaction)

$K_{Cr} = 478.9$ kJ mol^{-1} Å^{-2}	$r_C = 1.418$ Å
$K_{C\phi} = 562.2$ kJ mol^{-1}	$\theta_C = 120.00°$
$K_{C\phi}$[b] $= 25.12$ kJ mol^{-1}	$\gamma = 2.1867$ Å^{-1}
ϵ_{CC}[c] $= 0.4396$ kJ mol^{-1}	σ_{CC}[c] $= 3.851$ Å

[a] Ref 27 unless otherwise indicated. [b] This work. [c] Ref 31.

TABLE 2: Parameters for the Flexible (SPC) Water Model[a] and the Carbon−Water Potentials

$K_{Wr} = 4637$ kJ mol^{-1} Å^{-2}	$r_W = 1.0$ Å
$K_{W\theta} = 383$ kJ mol^{-1} rad^2	$\theta_W = 109.47°$
$\epsilon_{OO} = 0.6502$ kJ mol^{-1}	$\sigma_{OO} = 3.166$ Å
$q_O = -0.82$ e	$q_H = -0.41$ e
ϵ_{CO}[b] $= 0.3126$ kJ mol^{-1}	σ_{CO}[b] $= 3.19$ Å
$\Theta_{x'x'}$[c] $= -3.03 \times 10^{-40}$ C^2	

[a] Flexible water model, ref 1, unless otherwise indicated. [b] Ref 40. [c] Ref 52.

respectively. This model was found to predict the properties of subcritical[32] and supercritical[33−36] water in resonable agreement with experimental data.

Nonbonded interactions between the water molecules are comprised of a Lennard-Jones term between the oxygen atoms, cf. eq 4, and a Coulomb potential

$$U(r_{ij}) = \frac{1}{4\pi\epsilon_0}\frac{q_i q_j}{r_{ij}} \tag{6}$$

where ϵ_0 is the permittivity in a vacuum, and q_i, q_j are the partial charges, $q_O = -0.82$ and $q_H = 0.41$, respectively.[1] The Coulomb interaction is computed using a smooth truncation as

$$U(r_{ij}) = \frac{1}{4\pi\epsilon_0}\left(\frac{q_i q_j}{r_{ij}} - E_s(r_{ij})\right) \tag{7}$$

where $E_s(r_{ij})$ is a smoothing function

$$E_s(r_{ij}) = \frac{q_i q_j}{r_c} - (r_{ij} - r_c)\frac{q_i q_j}{r_c^2} \tag{8}$$

and r_c the radius of truncation.[37] The truncation of the Coulomb potential has been shown to have little effect on the thermodynamic and structural properties of bulk water for cutoffs larger than 6 Å,[38] and in this study we employ a value of 9.50 Å ($3\sigma_{OO}$) unless otherwise specified. The parameters of the potentials are summarized in Table 2.

2.1.3. Carbon−Water Interaction. The carbon−water interaction consists of a Lennard-Jones term between the carbon and oxygen atoms (eq 4) where the parameters of the potential, ϵ_{CO} and σ_{CO} are obtained from Bojan and Steele,[40] and a quadrupole interaction between the carbon atoms and the partial charges on the water hydrogen and oxygen atoms

$$U(\boldsymbol{r}) = \frac{1}{3}\frac{q}{4\pi\epsilon_0}\sum_{\alpha,\beta}\Theta_{\alpha,\beta}\frac{3r_\alpha r_\beta - r^2\delta_{\alpha\beta}}{r^5} \tag{9}$$

where α, β run over all Cartesian coordinates x, y, z, and r is the distance between an O or H charge site and the quadrupole carbon site. $\delta_{\alpha\beta}$ is the delta function, and $\Theta_{\alpha,\beta}$ is the quadrupole moment tensor.[39]

TABLE 3: Simulation Cases for a Carbon Nanotube in Water (CNT), Bulk (B), and Slab (S) Simulations of Water, and Carbon Nanotubes in Vacuum (V) [(m, n) are CNT indices; R the CNT radius; QP indicates inclusion of CNT quadrupole moment term; N_W and N_C are number of water molecules and carbon atoms, respectively; t_m is the total simulation time; and r_c the long-range potential cutoff distance.]

case	(m, n)	R (Å)	QP	N_W	N_C	t_m (ps)	r_c (Å)	type
1	(16,0)	6.26	no	2088	832	39	9.50	CNT
2	(16,0)	6.26	yes	2088	832	39	9.50	CNT
3	(16,0)	6.26	no	2088	832	39	12.66	CNT
4				729	0	62	9.50	B
5				729	0	94	9.50	S
6	(16,0)	6.26			832	6	9.50	V
7	(8,0)	3.15			416	11	9.50	V
8	(12,0)	4.71			624	6	9.50	V
9	(20,0)	7.83			1040	16	9.50	V
10	(10,10)	6.76			880	6	9.50	V

In the present study, we evaluate eq 9 in a local coordinate system (x', y', z') centered at the quadrupole site, cf. Figure 1. Thus, letting $\boldsymbol{x}'$ denote the wall normal direction, then

$$\Theta_{x'x'} = -2\Theta_{y'y'} = -2\Theta_{z'z'} \tag{10}$$

with all other components equal to zero, cf. ref 39. The quadrupole interaction is truncated at $r = r_c$, where r_c is the cutoff radius of the Lennard-Jones and Coulomb potentials. Note, that the effect of the quadrupole moment is an attraction of positive charge (hydrogen) toward the nanotube, and, conversely, a repulsion of negative charge (oxygen). Though the interaction was found to have only a minor effect on the adsorption of oxygen on graphite,[40] it can influence the orientation of the water at the interface. The parameters for the carbon−water potentials are summarized in Table 2.

3. Results

Molecular dynamics trajectories were computed for an infinite zigzag (16,0) carbon nanotube with radius 6.26 Å in water. Three cases were considered: case 1 without including the carbon quadrupole moment term in the potential and using a cutoff of 9.50 Å for the Coulomb and Lennard-Jones potentials ($3\sigma_{OO}$); case 2 with the same long-range cutoff and including the quadrupole moment term; and case 3 using a cutoff of 12.66 Å ($4\sigma_{OO}$) without including the quadrupole moment term. In addition two water MD trajectories were computed: case 4 bulk liquid water, and case 5 a liquid water slab with liquid−vapor interfaces in the $\pm x$ directions. Both water trajectories used a long-range cutoff of $3\sigma_{OO}$. Finally MD trajectories from 5 different nanotubes in a vacuum were also computed. The characteristics of all the MD trajectories are given in Table 3.

The structure of the CNT−water interface is presented in terms of the water radial density profile and the probability density profiles of the orientation of the water dipole moment ($P_r(\cos_i \varphi)$), the orientation of the OH bonds ($P_r(\cos_i \psi)$), and the orientation of the HOH plane of the water ($P_r(\cos_i \alpha)$) (see Figure 1), where

$$P_r(\cos_i \varphi) = \frac{\langle \cos_i \varphi \rangle_r + 1}{2}$$

$$P_r(\cos_i \psi) = \frac{\langle \cos_i \psi \rangle_r + 1}{2} \tag{11}$$

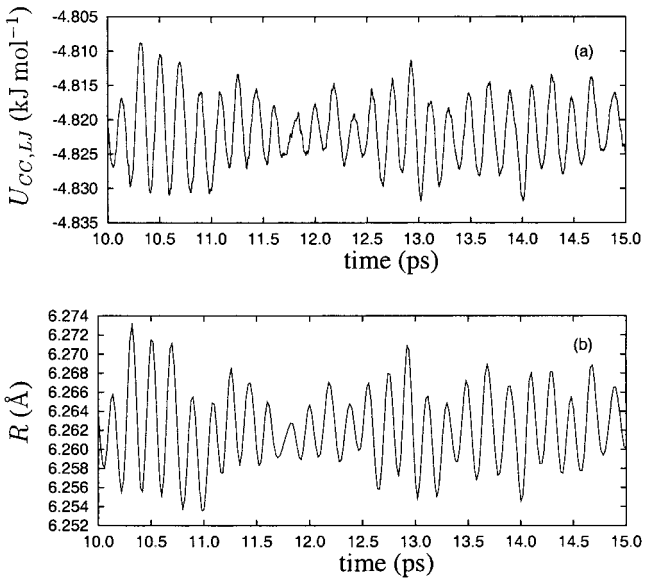

Figure 2. Time history of the (a) potential energy of the carbon−carbon Lennard-Jones interaction energy and (b) the radius of the CNT (case 1) displaying the breathing mode of the carbon nanotube in water.

and $\langle \cos_i \varphi \rangle_r$ and $\langle \cos_i \psi \rangle_r$ denote the average values of the cosine to the angle between the tangential plane of the CNT and the water dipole moment (φ) and the OH bond (ψ) of the ith bin at a radial position r. The planar symmetry of the water allows

$$P_r(\cos_i \alpha) = \langle |\cos_i \alpha| \rangle_r \qquad (12)$$

and α is the angle between the tangential plane and the plane of a water molecule.

The hydrogen bond structure is given in terms of the average number of hydrogen bonds per water molecule (n_{HB}) and is determined using a geometrical criterion.[41] Thus two water molecules are considered hydrogen-bonded if all the following conditions are satisfied:

(1) The distance between the oxygen atoms of both molecules is smaller than 3.6Å.

(2) The distance between the oxygen of the acceptor molecule and the hydrogen of the donor is less than 2.4 Å.

(3) The bond angle between the oxygen−oxygen direction and the molecular oxygen−hydrogen bond of the donor is less than 30°.

The statistics are collected every 20 fs until 39 ps, with a total of 1800 samples. The radial profiles are sampled in 60 bins of constant volume extending from the surface of the carbon nanotube.

3.1. Properties of the Carbon Nanotube. The molecular dynamics simulations of the carbon nanotube in water revealed a persistent oscillation of the carbon−carbon Lennard-Jones interaction energy ($\boldsymbol{U}_{CC,\,LJ}$) with a frequency of 173 cm^{-1}, cf. Figure 2a. As this value is close to the result of tight binding calculations for the frequency of the first radial mode (the "breathing mode", A_{1g}) of this carbon nanotube in a vacuum (179 cm^{-1}),[26] additional simulations of nanotubes in a vacuum were carried out (cases 6−10, cf. Table 3) to estimate the accuracy of the present force field to simulate the dynamic behavior of the CNT. In these simulations the first radial mode was excited by assigning an initial radial velocity to the carbon atoms corresponding to a kinetic energy of 0.07 kJ mol^{-1}. The radius of the carbon nanotube was found to oscillate with an amplitude of approximately 1% of the mean radius, and with a frequency corresponding to that observed for the oscillation of the carbon−carbon Lennard-Jones potential energy, cf. Figure 2b for the CNT in water.

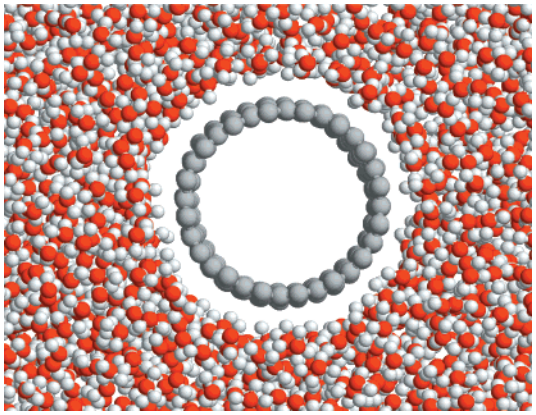

Figure 3. Snapshot of the atoms for the simulation of a carbon nanotube in water. The interaction potentials include an electrostatic quadrupole moment (case 2).

TABLE 4: Breathing Frequency (in cm^{-1}) of Carbon Nanotubes in Water (case 1) and in Vacuum (cases 6−9), Compared with Tight-binding Molecular Dynamics Simulations,[26,42] Experimental Results,[43] and First Principle Calculations[44,45]

case	(*m*,*n*)	*R* (Å)	present	ref 26	ref 42	expt	refs 44, 45
1	(16,0)	6.26	174				
6	(16,0)	6.26	173	179	170	≈173	188
7	(8,0)	3.15	351	356			
8	(12,0)	4.71	232	238	226		
9	(20,0)	7.83	139	143			150
10	(10,10)	6.76	160	166	157	≈165	175

The predicted breathing frequencies are compared with results from tight-binding molecular dynamics simulations of Saito et al.[26] and Kahn and Lu,[42] with the experimental results of Duesberg et al.,[43] and with the ab initio calculations of Kürti et al.[44] and Sánchez-Portal et al.,[45] cf. Table 4. The well-known inverse relationship between the radius of the CNT and the breathing frequency is predicted to within 4% of these previous studies with a calculated proportionality constant of 1120 cm^{-1} Å. The value of the predicted frequency is generally lower than values from ab initio calculations, but in good agreement with the experimental data.[43,46] By comparing the breathing frequency of the CNT in water (case 1) and vacuum (case 6) we conclude that the influence of the water on the breathing mode is negligible (Table 4).

3.2. Properties of the Water−Nanotube Interface. The structural properties of the water−carbon nanotube interface are studied by examination of the water radial density profile, water orientation, and hydrogen bond profiles for cases 1−3. The water molecules stand off from the nanotube by approximately 3.2 Å as seen in Figure 3. For comparison, the results of bulk liquid water and water slab simulations, with planar liquid-vapor interfaces, are used.

3.2.1. Water Density Profiles. The radial density profiles for the hydrogen and oxygen atoms are shown in Figure 4a and b, for the simulations of a carbon nanotube in water excluding and including the quadrupole moment, respectively. The maxima of the oxygen and hydrogen profiles at a radial distance $r^* \equiv r - R$ of 3.20 Å (corresponding to the value of σ_{CO}) nearly coincide indicating that the plane of the water molecules is approximately tangential to the cylindrical CNT−water interface. The thickness of the profiles as defined by the extent of the density variations is 6−7 Å, comparable to the thickness of

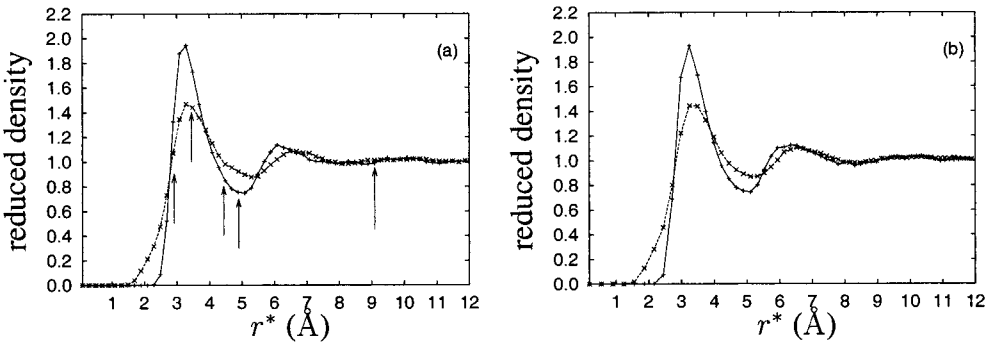

Figure 4. Water radial density profile. The arrows indicate the centers of the bins used in the water dipole moment distribution (Figure 6). (a) Excluding the quadrupole moment; (b) including the quadrupole moment. $-+-$: oxygen density profile (ρ_O/ρ_O^0); $-\times-$: hydrogen density profile (ρ_H/ρ_H^0), where ρ_O^0 and ρ_H^0 are the bulk oxygen and hydrogen densities, respectively.

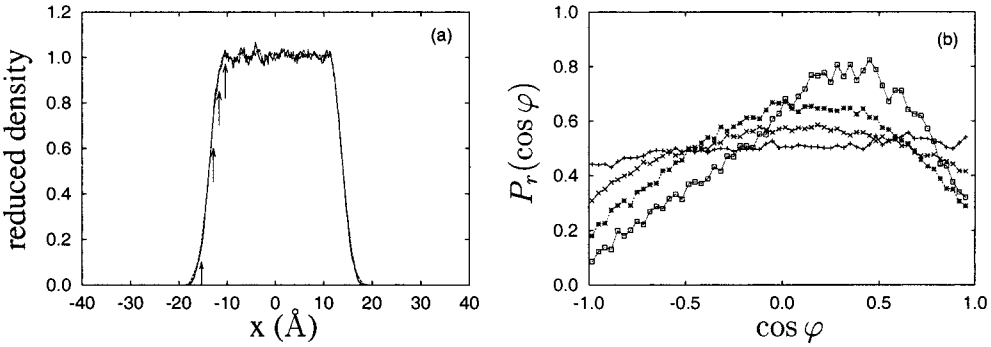

Figure 5. Water density profile (a) and orientation of the water dipole moment (b) for a slab of water. The density profiles (—: oxygen, and $--$: hydrogen) are collected in bins of width 0.154 Å. The arrows in (a) indicate the centers of the bin shown in (b) $-\square-$: $x = -15.31$ Å; $-*-$: $x = -12.85$ Å; $-\times-$: $x = -11.62$ Å; $-+-$: $x = -10.39$ Å.

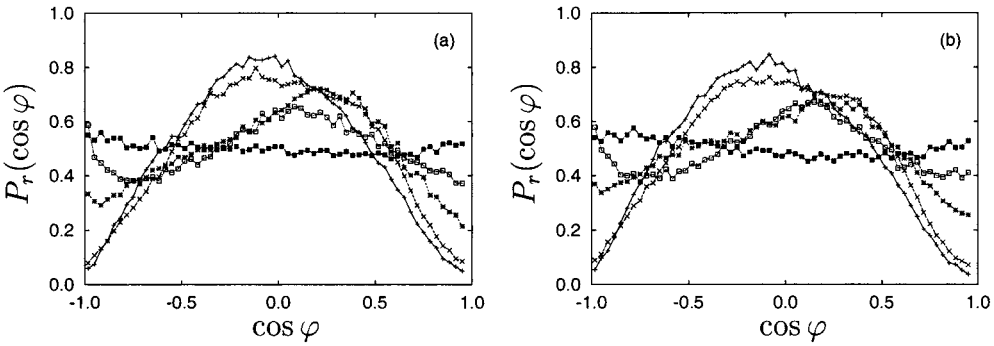

Figure 6. Orientation of the water dipole moment at different radial distances from the carbon nanotube wall. (a) Quadrupole moment excluded; (b) quadrupole moment included. $-+-$: $r^* = 2.85$ Å; $-\times-$: $r^* = 3.37$ Å (first peak); $-*-$: $r^* = 4.34$ Å; $-0-$: $r^* = 4.79$ Å (first minimum); $-\blacksquare-$: $r^* = 8.89$ Å (bulk phase).

the planar liquid−vapor interface, cf. Figure 5, but in the presence of the carbon nanotube the water density profile displays a characteristic layering and distinct presence of hydrogen atoms closer to the nanotube, i.e., for $r^* < 2.1$ Å.

These density profiles are, in general, in good agreement with the study of Wallqvist[47] for polarizable water in contact with a smooth wall, and with grand canonical Monte Carlo simulations of water adsorption in graphite pores by Ulberg and Gubbins.[12] The influence of the quadrupole moment on the density is clearly small.

3.2.2. Orientation of Water Molecules. The orientation of the water molecules at the CNT−water interface can be inferred from the orientation of the water dipole moment, cf. Figure 6. The water molecules in closest proximity to the CNT (at $r^* = 2.85-3.37$ Å) display a preference for angles of $\varphi = 94°-95°$ indicating that the dipole moment is nearly tangential to the plane of the CNT. At a radial distance of 4.90 Å, corresponding to the point of local minimum density, the dipole moment has turned to an angle of 75°, thus pointing in the direction of the bulk. The bulk properties are finally reached at $r^* \geq 9.00$ Å. These results are in good agreement with the study of water between hydrophobic surfaces by Lee et al.,[48] and with the work of Wallqvist.[47]

To further study the orientation of the water molecules we consider the orientation of the OH bonds as shown in Figure 7. At a radial distance of 2.85 Å the OH bonds are nearly tangential to the plane of the CNT, exhibiting an angle of $\psi = 92°-93°$. The point of maximum probability shifts from this nearly parallel configuration to an orientation of 100°, 115°, 125°, and 135° at a radial distance of 3.37, 4.34, 4.79, and 5.22 Å, respectively. This corresponds to a rotation of the HOH plane toward the perpendicular to the interface. This conclusion is confirmed by considering the orientation of the HOH plane as shown in Figure 8. The HOH plane of the water has a slightly elevated probability of 90° at $r^* = 6.04$ Å corresponding to the second peak in the oxygen density profile. The OH profiles (see Figure

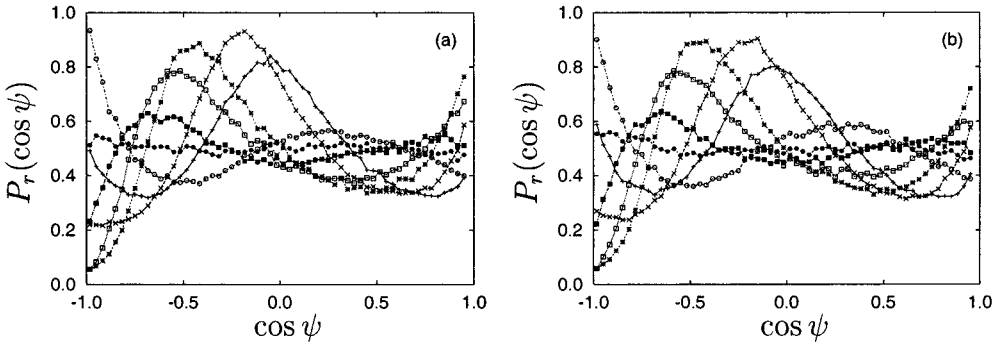

Figure 7. Orientation of the OH bonds at different distances from the carbon nanotube wall. (a) Quadrupole moment excluded; (b) quadrupole moment included. −+−: $r^* = 2.85$ Å; −×−: $r^* = 3.37$ Å (first peak); −∗−: $r^* = 4.34$ Å; −□−: $r^* = 4.79$ Å (first minimum); −■−: $r^* = 5.22$ Å; −○−: $r^* = 6.04$ Å (second peak); −●−: $r^* = 8.89$ Å (bulk phase).

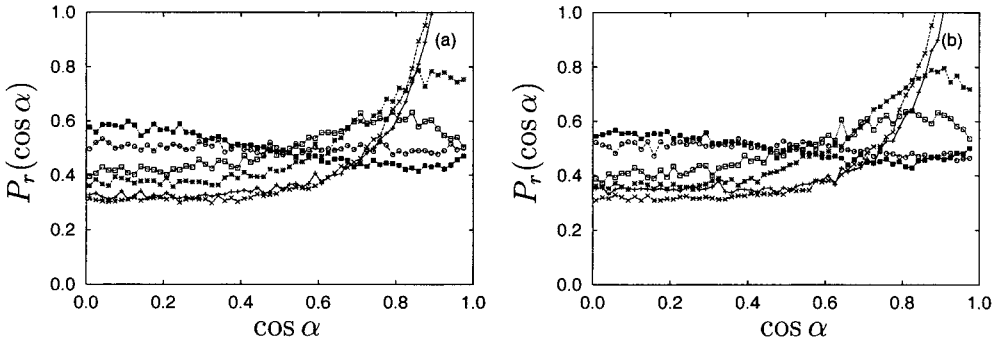

Figure 8. Orientation of the HOH plane at different distances from the carbon nanotube wall. (a) Quadrupole moment excluded; (b) quadrupole moment included. −+−: r* = 2.85 Å; −×−: $r^* = 3.37$ Å; −*−: $r^* = 4.34$ Å; −□−: $r^* = 4.79$ Å; −■−: $r^* = 6.04$ Å; −○−: $r^* = 8.89$ Å.

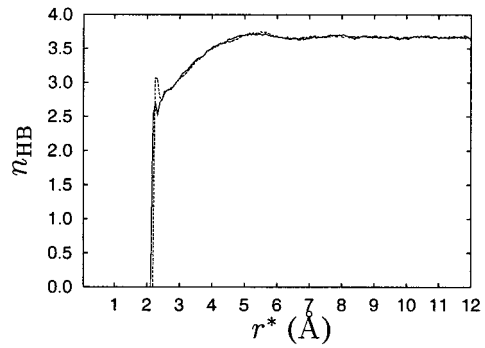

Figure 9. Radial profiles of the hydrogen bond population, expressed as the average number of hydrogen bonds per water molecule (n_{HB}). —: quadrupole moment excluded; − − −: quadrupole moment included.

7) clearly indicate the presence of the second OH bond with elevated probabilities for 25° and 75° (the OH bond pointing toward the bulk) at a radial distance of 5.22 and 6.04 Å, respectively. From Figures 7 and 8 we again observe a negligible influence of the quadrupole moment.

Finally, we show the modification of the water hydrogen bonds structure in the vicinity of the CNT in Figure 9. For both simulations including and excluding the quadrupole moment we find that the average number of hydrogen bonds decreases from a bulk value of 3.75 to a value of 2.89 at the CNT−water interface. The initial peak in the profiles at $r^* = 2.2-2.3$ is caused by poor sampling. In addition we observe a small decrease to a value of 3.64 around the second peak in the water density profile ($r^* = 6-7$ Å). These profiles are in general in good agreement with the study of Lee et al.[48]

The spherical truncation of long-range potentials in inhomogeneous systems can introduce errors due to a reduction of the charge screening. An additional simulation (case 3) was performed using a larger cutoff radius (12.66 Å) to investigate this effect under the present conditions. The radial density profile and the dipole moment are shown in Figure 10 for the two cases (cases 1 and 3). The root-mean square difference between the profiles are less than 2%, and 5% for the density and dipole moment profiles, respectively. Thus, in the present case, a cutoff value of 9.50 Å appears to be sufficient.

3.3. Energetics. The results of the CNT−water simulation can be used to analyze the energetic aspects associated with the process of introducing a CNT from the gas phase into aqueous solution. The total energy change in this process, denoted by $\Delta E_{g\to w}$, has three main contributions:

$$\Delta E_{g\to w} = \Delta E_{CC} + \Delta E_{CW} + \Delta E_{WW} \qquad (13)$$

Here, ΔE_{CC} represents the change in energy coming from interactions among carbon atoms. This is primarily due to the presence of water molecules surrounding the CNT that slightly alters the C−C interactions. In general, this contribution is expected to be small. ΔE_{CW} is the energy arising from interactions between the carbon atoms of the nanotube and the surrounding water molecules. The ΔE_{WW} part represents the energy required to create a cavity in water to accommodate the CNT. This contribution is due to interactions between water molecules and is related to the surface energy which will be analyzed below. For the system considered here, the energy changes (in kJ mol^{-1} per length of the CNT in Å) are calculated as: $\Delta E_{CC} = 0.59$, $\Delta E_{CW} = -17.33$, and $\Delta E_{WW} = 45.40$, producing $\Delta E_{g\to w} = 28.66$ kJ mol^{-1}. These results show that the energy contribution coming from C−C interactions is positive and quite small with respect to other contributions, as expected. The interactions between carbon atoms and the surrounding water molecules are attractive and fairly large. However, the ΔE_{WW} part has a positive value and it is the largest

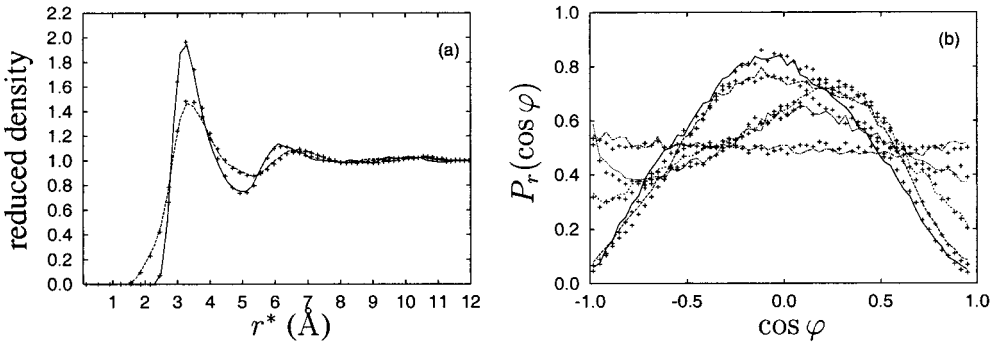

Figure 10. Water radial density profile (compare to Figure 4) (a) and the dipole moment (b) using the reference cutoff radius of 9.50 Å (—) and a cutoff radius of 12.66 Å (+++), respectively. In (b), same number of bins are used as in Figure 6.

contribution. The net result, clearly indicates that the process of introducing a CNT in an aqueous solution is energetically unfavorable.

We analyze further the ΔE_{WW} component, which is the most important contribution to the CNT solvation energy, and reflects surface characteristics and the surface energy associated with the cavity creation in water. To compare present results with experiments, we first calculate the energy for a flat surface of water. The surface energy is determined from the difference between the energies (per water molecule) calculated for bulk and slab water simulation, cases 3 and 4 shown in Table 3. The bulk water simulation contains 729 water molecules confined in a three-dimensional periodic box. For the slab, the periodic boundaries in one direction were removed, creating two exposed surfaces. The bulk calculation yields an average potential energy value of -41.90 ± 0.18 kJ mol^{-1}. This represents a bulk water environment corresponding to a density of 997 kg m^{-3} at $T = 300$ K and $P = 1$ atm. For the slab system with exposed surfaces (case 5) the average energy is determined to be -40.28 ± 0.16 kJ mol^{-1}. For this case, the exposed surface area is 1582.6 Å^2. This analysis for the bulk and slab water models yields a surface energy value of 124 ± 25 dynes/cm. There is a relatively large deviation from the mean value, but this is not unexpected considering the small size of the system. Nevertheless, this value of the average surface energy calculated for pure water is in good agreement with the experimental surface energy for pure water, 119.66dynes/cm,[49,50] which was obtained from the experimental surface tension of water and its temperature dependence around 300 K.

Next, we consider the surface energy for the cavity accommodating the carbon nanotube. Here, the difference between the energy of bulk water and ΔE_{WW} reflects the surface energy of the cavity. The radius of the cylindrical cavity is taken as 9.46 Å, the distance from the CNT axis to the first peak in the water radial density shown in Figure 4a. This analysis yields an average surface energy of 126.9dynes/cm for the cylindrical cavity created in water. In this case also, the deviation from the mean ($\approx \pm 25$ dynes/cm) is the same as found for the flat surface indicated above. Thus, the surface energy calculated here for the cylindrical surface is comparable to the surface energy calculated for the planar surface.

Present results indicate that small configurational changes in the water orientation do not affect the surface energy greatly. Furthermore, the curved surface here represents a carbon nanotube/water interface while the planar surfaces of water are facing a vacuum. According to the present outcome, the surface energy does not show any appreciable dependence of the nature and geometry of the surface. The result agrees with earlier studies concluding that curvature effects are operational only at extremly small radii.[51]

4. Summary and Conclusions

We have presented molecular dynamics simulations of the structure of water in the interface external to a carbon nanotube. Using a detailed description of the carbon nanotube and classical potentials for the carbon−water interaction including an electrostatic quadrupole moment acting between the carbon atoms and the charge sites on the water, we find structural properties of water similar to those found for water at an idealized graphite surface. However, in the present case, the plane of the water molecules is slightly inclined toward the CNT with an angle of the dipole moment of 94°−95°. The quadrupole moment was found to have a negligible influence of the structural properties of the water.

The breathing mode of the CNT can be inferred from the van der Waals carbon−carbon interaction energy and the breathing frequency was found in good agreement with experimental data. The presence of the water was found to have a negligible influence on the breathing frequency at the present conditions.

Finally, we considered the process of introducing a CNT into water. In this process, energy changes coming from carbon−carbon, carbon−water, and water−water interactions were calculated and analyzed separately. The water−water interactions which reflect the cavity creation energy are found to be the most important contribution. Also, we investigated the energetics calculated for a flat surface of water facing a vacuum, and for the cylindrical cavity surface facing the CNT. In these cases, the surface energies were found to be quite comparable, despite some differences in the orientation of dipole moments. Furthermore, the calculated energy for flat surfaces of water agrees well with the experimental value.

Acknowledgment. We acknowledge discussions with Andrew Pohorille, Michael Wilson, and Michael New at NASA Ames Computational Astrobiology Branch, with Christopher Dateo at the NASA Ames Computational Chemistry Branch, and with Flavio Noca from the Jet Propulsion Laboratory. Support for T.H. is provided by NASA contract NAS2-9902 to ELORET corporation. The support from the Research Commission at ETH Zürich, and from the CTR Summer Program 2000 Stanford University is greatly appreciated.

References and Notes

(1) Teleman, O.; Jönsson, B.; Engström, S. *Mol. Phys.* **1987**, *60* (1), 193−203.

(2) Odom, T. W.; Huang, J.-L.; Kim, P.; Lieber, C. M. *J. Phys. Chem. B* **2000**, *104*, 2794−2809.

(3) Balavoine, F.; Schultz, P.; Richard, C.; Mallouh, V.; Ebbesen, T. W.; Mioskowski, C. *Angew. Chem.* **1999**, *38* (13/14), 1912−1915.

(4) Jarvis, S. P.; Uchihashi, T.; Ishida, T.; Tokumoto, H.; Nakayama, Y. *J. Phys. Chem. B* **2000**, *104* (26), 6091−6094.
(5) Moloni, K.; Buss, M. R.; Andres, R. P. *Ultramicroscopy* **1999**, *80*, 237−246.
(6) Li, J.; Cassell, A. M.; Dai, H. *Surf. Interface Anal.* **1999**, *28*, 8−11.
(7) Wang, Q.; Johnson, J. K. *J. Phys. Chem. B* **1999**, *103*, 4809−4813.
(8) Rzepka, M.; Lamp, P.; de la Casa-Lillo, M. A. *J. Phys. Chem. B* **1998**, *102*, 10894−10898.
(9) Gordon, P. A.; Saeger, R. B. *Ind. Eng. Chem. Res.* **1999**, *38*, 4647−4655.
(10) Lee, S. M.; Lee, Y. H. *Appl. Phys. Lett.* **2000**, *76* (20), 2877−2879.
(11) Müller, E. A.; Rull, L. F.; Vega, L. F.; Gubbins, K. E. *J. Phys. Chem.* **1996**, *100* (4), 1189−1196.
(12) Ulberg, D.; Gubbins, K. E. *Mol. Phys.* **1995**, *84* (6), 1139−1153.
(13) Allen, T. W.; Kuyucak, S.; Chung, S.-H. *J. Chem. Phys.* **1999**, *111* (17), 7985−7999.
(14) Shevade, A. V.; Jiang, S.; Gubbins, K. E. *Mol. Phys.* **1999**, *97* (10), 1139−1148.
(15) Dujardin, E.; Ebbesen, T. W.; Hiura, H.; Tanigaki, K. *Science* **1994**, *265*, 1850−1852.
(16) Dujardin, E.; Ebbesen, T. W.; Krishnan, A.; Treacy, M. M. J. *Adv. Mater.* **1998**, *10* (17), 1472−1475.
(17) Scrivens, W. A.; Tour, J. M. *J. Chem. Soc., Chem. Commun.* **1993**, 1207−1209.
(18) Ruoff, R. S.; Tse, D. S.; Malhotra, R.; Lorents, D. C. *J. Phys. Chem.* **1993**, *97*, 3379−3383.
(19) Liu, J.; Rinzler, A. G.; Dai, H.; Hafner, J. H.; Bradley, R. K.; Boul, P. J.; Lu, A.; Iverson, T.; Shelimov, K.; Huffman, C. B.; Rodriguez-Macias, F.; Shon, Y.-S.; Lee, T. R.; Colbert, D. T.; Smalley, R. E. *Science* **1998**, *280*, 1253−1256.
(20) Chen, J.; Hamon, M. A.; Hu, H.; Chen, Y.; Rao, A. M.; Eklund, P. C.; Haddon, R. C. *Science* **1998**, *282*, 95−98.
(21) Hamon, M. A.; Chen, J.; Hu, H.; Chen, Y.; Itkis, M. A.; Rao, A. M.; Eklund, P. C.; Haddon, R. C. *Adv. Mater.* **1999**, *11* (10), 834−840.
(22) Mickelson, E. T.; Chiang, I. W.; Zimmerman, J. L.; Boul, P. J.; Lozano, J.; Liu, J.; Smalley, R. E.; Hauge, R. H.; Margrave, J. L. *J. Phys. Chem. B* **1999**, *103*, 4318−4322.
(23) Vernov, A.; Steele, W. A. *Langmuir* **1992**, *8*, 155−159.
(24) Marković, N.; Andersson, P. U.; Någård, M. B.; Petterson, J. B. C. *Chem. Phys.* **1999**, *247*, 413−430.
(25) Marković, N.; Andersson, P. U.; Någård, M. B.; Petterson, J. B. C. *Chem. Phys.* **2000**, *252*, 409−410.
(26) Saito, R.; Takeya, T.; Kimura, T.; Dresselhaus, G.; Dresselhaus, M. S. *Phys. Rev. B* **1998**, *57* (7), 4145−4153.
(27) Guo, Y.; Karasawa, N.; Goddard, W. A. III. *Nature* **1991**, *351*, 464−467.
(28) Tuzun, R. E.; Noid, D. W.; Sumpter, B. G.; Merkle, R. C. *Nanotech.* **1996**, *7* (3), 241−248.
(29) Frisch, M. J.; Trucks, G. W.; Schlegel, H. B.; Scuseria, G. E.; Robb, M. A.; Cheeseman, J. R.; Zakrzewski, V. G.; Montgomery, J. A., Jr.; Stratmann, R. E.; Burant, J. C.; Dapprich, S.; Millam, J. M.; Daniels, A. D.; Kudin, K. N.; Strain, M. C.; Farkas, O.; Tomasi, J.; Barone, V.; Cossi, M.; Cammi, R.; Mennucci, B.; Pomelli, C.; Adamo, C.; Clifford, S.; Ochterski, J.; Petersson, G. A.; Ayala, P. Y.; Cui, Q.; Morokuma, K.; Malick, D. K.; Rabuck, A. D.; Raghavachari, K.; Foresman, J. B.; Cioslowski, J.; Ortiz, J. V.; Stefanov, B. B.; Liu, G.; Liashenko, A.; Piskorz, P.; Komaromi, I.; Gomperts, R.; Martin, R. L.; Fox, D. J.; Keith, T.; Al-Laham, M. A.; Peng, C. Y.; Nanayakkara, A.; Gonzalez, C.; Challacombe, M.; Gill, P. M. W.; Johnson, B. G.; Chen, W.; Wong, M. W.; Andres, J. L.; Head-Gordon, M.; Replogle, E. S.; Pople, J. A. *Gaussian 98*, revision A.7; Gaussian, Inc.: Pittsburgh, PA, 1998.
(30) Becke, A. D. *J. Chem. Phys.* **1993**, *98*, 5648−5652.
(31) Rappé, A. K.; Casewit, C. J.; Colwell, K. S.; Goddard W. A., III; Skiff, W. M. *J. Am. Chem. Soc.* **1992**, *114*, 10024−10035.
(32) Wallqvist, A.; Teleman, O. *Mol. Phys.* **1991**, *74* (3), 515−533.
(33) Mizan, T. I.; Savage, P. E.; Ziff, R. M. *J. Phys. Chem.* **1994**, *98*, 13067−13076.
(34) Mizan, T. I.; Savage, P. E.; Ziff, R. M. *J. Comput. Chem.* **1996**, *17* (15), 1757−1770.
(35) Mizan, T. I.; Savage, P. E.; Ziff, R. M. *J. Phys. Chem.* **1996**, *100*, 403−408.
(36) Mizan, T. I.; Savage, P. E.; Ziff, R. M. *J. Supercrit. Fluids* **1997**, *10*, 119−125.
(37) Levitt, M.; Hirshberg, M.; Laidig, K. E.; Daggett, V. *J. Phys. Chem. B* **1997**, *101*, 5051−5061.
(38) Andrea, T. A.; Swope, W. C.; Andersen, H. C. *J. Chem. Phys.* **1984**, *79* (9), 4576−4584.
(39) Hansen, F. Y.; Bruch, L. W. *Phys. Rev. B* **1995**, *51* (4), 2515−2536.
(40) Bojan, M. J.; Steele, W. A. *Langmuir* **1987**, *3* (6), 1123−1127.
(41) Gordillo, M. C.; Martí, J. *Chem. Phys. Lett.* **2000**, *329*, 341−345.
(42) Kahn, D.; Lu, J. P. *Phys. Rev. B* **1999**, *60* (9), 6535−6540.
(43) Duesberg, G. S.; Blau, W. J.; Byrne, H. J.; Muster, J.; Burghard, M.; Roth, S. *Chem. Phys. Lett.* **1999**, *310*, 8−14.
(44) Kürti, J.; Kresse, G.; Kuzmany, H. *Phys. Rev. B* **1998**, *58* (14), R8869−R8872.
(45) Sánchez-Portal, D.; Artacho, E.; Soler, J. M.; Rubio, A.; Ordejón, P. *Phys. Rev. B* **1999**, *59* (19), 12678−12688.
(46) Rao, A. M.; Richter, E.; Shunji, B.; Chase, B.; Eklund, P. C.; Williams, K. A.; Fang, S.; Subbaswamy, K. R.; Menon, M.; Thess, A.; Smalley, R. E.; Dresselhaus, G.; Dresselhaus, D. M. *Science* **1997**, *275*, 187−191.
(47) Wallqvist, A. *Chem. Phys. Lett.* **1990**, *165* (5), 437−442.
(48) Lee, C. Y.; McCammon, J. A.; Rossky, P. J. *J. Chem. Phys.* **1984**, *80* (9), 4448−4455.
(49) Lide, D. R. *Handbook of Chemistry and Physics*, 78th ed.; CRC Press: New York, 1998.
(50) Kroschwitz, J. I., Howe-Grant, M., Eds. *Encyclopedia of Chemical Technology*, 4th ed.; New York, 1998.
(51) Bogdan, A. *J. Chem. Phys.* **1997**, *106* (5), 1921−1929.
(52) Whitehouse, D. B.; Buckingham, A. D. *J. Chem. Soc., Faraday Trans.* **1993**, *89* (12), 1909−1913.